25th ABCM International Congress of Mechanical Engineering
October 20-25, 2019, Uberlândia, MG, Brazil

COB-2019-0665
EULER-LAGRANGE 3D SIMULATION OF ETHANOL INJECTED IN A QUIESCENT AIR CHAMBER

Bruno Silva de Lima
Francisco José de Souza
Universidade Federal de Uberlândia, School of Mechanical Engineering, Federal University of Uberlândia, João Naves de Ávila Avenue, 2121, bloco 5P, Uberlândia 38400-902, Minas Gerais, Brazil
brunosilvadelima@hotmail.com
francisco.souza@ufu.br

Rafael Silva de Lima
Federal University of Itajubá - campus Itabira, Irmã Ivone Drumond street, 200, Distrito Industrial II, Itabira, CEP 35903-087, Minas Gerais, Brazil
rafaelsilvadelima37@gmail.com

Abstract. *A well-controlled fuel mixture process inside engines leads to a system improvement as a whole, thus, it is necessary to understand the interaction between air and fuel. To characterize an injection, the first step is testing it in a quiescent air chamber. Due to the complexity of this process, the prediction of injection behavior inside the chamber is carried out using computational tools. In the literature there are some models to predict the breaking of the liquid jet into droplets as well as its atomization. In the present work the KH-RT as well as TAB break models are tested for an outwardly opening nozzle type injector to describe the Lagrangian phase at an injection pressure of 100 bar using the commercial CONVERGE software. To simulate the Eulerian phase, which is the air inside the chamber, the RNG-ke model is used to describe turbulence. To validate the simulation, the jet of ethanol in a quiescent air chamber at atmospheric pressure is compared to data found in the literature for the jet penetration. The results showed that the correlations are able to predict the results with good precision, although showing that the models tested overestimate the results experimentally obtained for fuel penetration.*

Keywords: *Spray, secondary breakup, CONVERGE, KH-RT, TAB*

1. INTRODUCTION

With the increase in the world's cars fleet, the efficiency and emission of pollutant gases from internal combustion engines becomes a concern of interest. To regulate the emission of pollutant gases, increasingly strict regulations are created. These regulations demand the improvement of the existent technologies as well as the development of new technologies to meet the new standards. (Baumgarten, 2006)

Renewable fuels, such as ethanol, have been used in substitution for fossil fuels to meet the needs imposed by the regulations that control the pollution standards. Their combustion process depend on the quality of the air fuel mixture, considering that a better atomization of the liquid implies in a better evaporation which leads to a more effective energy release and a lower concentration of polluting gases. (Baumgarten, 2006)

Before testing the fuel in the internal combustion engines the characterization of the spray is a necessary step. This step is carried out in a quiescent chamber and parameters such as spray penetration and cone angle can be experimentally measured or predicted using numerical correlations. Research related to this fuels has grown, and considering the complexity of the mixture of air and fuel, three dimensional numerical simulations have been used to study this process. (Baumgarten, 2006)

Within this context, the main purpose of this paper is to validate three break-up model correlations for an ethanol injection in a quiescent air chamber by means of an outwardly spray injector.

2. SPRAY MODELS

Sprays are essentially a liquid dispersion in a gaseous medium, which can be produced by means of different phenomena. To effectively produce a spray, it is necessary a high velocity difference between the liquid and the gaseous phase. (LEFEBVRE, 1989)

The main characteristics for a hollow cone spray are shown in Figure 1. It is important to note the liquid penetration S, which is the maximum distance from the end of the injector, that droplets can be found. This measurement is often used in the first steps of an engine project as well as used to validate break up models.

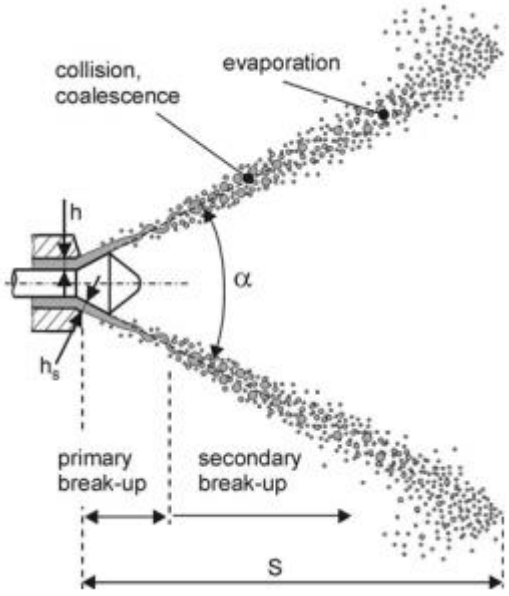

Figure 1 – Hollow cone spray (Baumgarten, 2006)

The atomization of the spray and the consequently vaporisation is characterized by the breakup phenomenon. The primary breakup is characterized by the transformation of the liquid jet in small drops. This first breakup is responsible for the initial conditions of the drop, such as its velocity and diameter. Ohnesorge studied these mechanisms and showed that there are four different breakup mechanisms dependent on the Ohnesorge number Eq. (3) (which is a combination of the Weber number Eq. (2) and Reynolds number Eq. (1)) and Weber number and are correlated as Shown in Figure 2. (Baumgarten, 2006)

$$R_e = \frac{uD\rho_l}{\mu_l} \tag{1}$$

$$W_{el} = \frac{u^2 D\rho_l}{\sigma} \tag{2}$$

$$Z = \frac{\sqrt{W_{el}}}{R_e} = \frac{\mu_l}{\sqrt{\sigma\rho_l D}} \tag{3}$$

Where u is the relative velocity, D is the droplet diameter, ρ_l is the liquid specific mass, μ_l is the dynamic viscosity and σ is the surface tension.

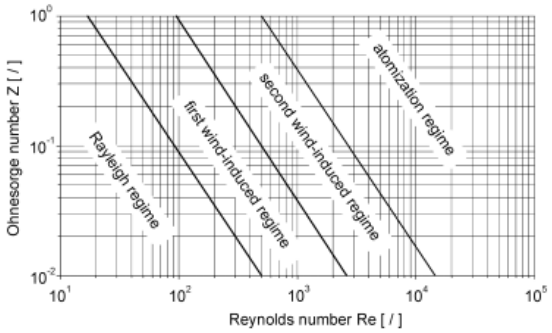

Figure 2 – Ohnesorg diagram (Baumgarten, 2006)

Considering the same fluid and the same injector and varying the velocity of the liquid all the mechanisms can be observed. At low velocities the Rayleigh regime is observed, in which the drops are formed from an unbroken jet. With a rise in the speed the first wind induced regime is found and it is characterized by stronger aerodynamic forces, which lead to a smaller unbroken jet and also smaller drops. In the second wind-induced regime the occurs due to the growth of short wavelength surface waves initiated by jet turbulence and amplified by aerodynamic forces due to the relative velocity between the liquid jet and the surrounding air. The atomization regime is reached if the unbroken jet is nearly zero, the spray breakup starts immediately when the liquid leaves the injector. The regimes are illustrated in Figure 3. (Baumgarten, 2006)

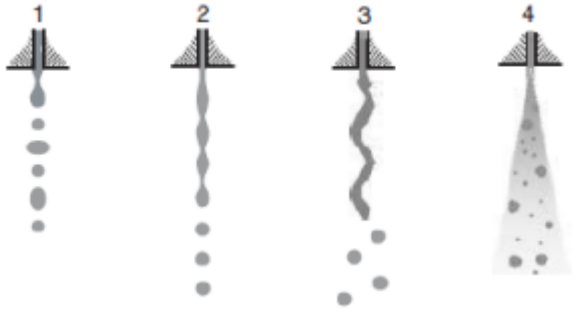

Figure 3 – Illustration of the breakup regimes (BRAVO & KWEON, 2014)

In the second breakup, liquid ligaments and droplets of the spray are subjected to a breakup caused by the aerodynamic forces and pressure, which are induced by the relative velocity between the droplets and the surrounding air. Aerodynamic forces promote unstable growth of the waves at the gas-liquid interface, which leads to breakup. Based on experimental investigations, it was noticed that the different secondary breakup regimens are dependent on the Weber number of the gas phase and different regimes are noticed as show in Figure 4, the greater the weber number the closer to catastrophic regime. (Baumgarten, 2006)

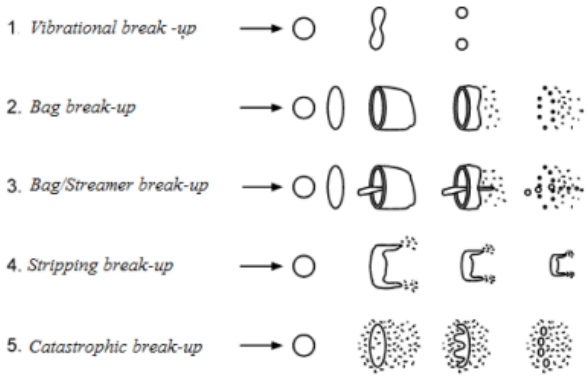

Figure 4 – Illustration of the breakup regimes (Baumgarten, 2006)

The next subsections briefly summarize how the breakup models are modeled for simulations here presented. More details are presented in (Richards et al, 2016).

2.1 TAB Spray Breakup Model

The Taylor Analogy Breakup model is used to calculate drop distortion and breakup. It is based on the analogy of an oscillating droplet and a spring-mass system. The governing equation for a damped and forced oscillating system is shown in Eq. (4). (Richards et al, 2016)

$$F - kx - d\dot{x} = m\ddot{x} \tag{4}$$

Where x is the displacement of the drop from its undisturbed position. Setting $y = x\,/C_b r_0$, where r_0 is the undisturbed droplet radius and C_b is a dimensionless constant defined as 0.5, the droplet oscillation frequency w and y can be expressed in Eq. (5) and (6). (Richards et al, 2016)

$$w^2 = C_k \frac{\sigma}{\rho_l r_0^3} + \frac{1}{{t_d}^2} \tag{5}$$

$$y(t) = We_c + e^{-t/t_d}\left[(y - We_c)\cos(wt) + \frac{1}{w}\left(\frac{dy}{dt}(0) + \frac{y(0) - We_c}{t_d}\right)\sin(wt)\right] \tag{6}$$

Where C_k is a dimensionless constant defined as 8, t_d is the turbulence correlation time and We_c is the drop Weber number.

If w^2 is greater than zero then the amplitude A is calculated by Eq. (7).(Richards et al, 2016)

$$A = \sqrt{(y - We_c)^2 + (y/w)^2} \tag{7}$$

If $A + We_c \leq 1$ the phenomenon is not observed. Otherwise if $A + We_c \geq 1$and $y \geq 1$ or the computational time step is larger than the breakup time, breakup is predicted to occur. (Richards et al, 2016)

2.2 KH-RT Spray Breakup Model

According to (Richards et al, 2016) the KH-RT model is a combination of the Kelvin-Helmholtz analogy for breakup with the Rayleigh-Taylor analogy developed by (Reitz and Diwakar, 1987). In this model both breakup models run simultaneously, the KH analogy is responsible for primary breakup in an intact core length *Lb* and for the second breakup a comparison of the effects of the KH and RT models is modeled as shown in Figure 5.

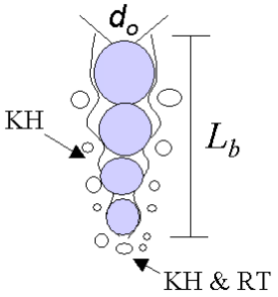

Figure 5 – KH-RT model (Richards et al, 2016)

The Kelvin-Helmholtz analogy is based on a liquid jet stability analysis, in which a liquid jet enters a quiescent chamber. An arbitrary displacement η is imposed in the system as shown by Eq. (8). (Richards et al, 2016)

$$\eta = \eta_0 e^{ikz + \omega t} \tag{8}$$

The linearized hydrodynamic equations are solved with wave solutions of the form shown in Eq. (9) and (10).

$$\phi_l = C_1 I_0(k_{KH} r) e^{ik_{KH} z + \omega_{KH} t} \tag{9}$$

$$\psi_l = C_2 r I_1(Lr) e^{ik_{KH} z + \omega_{KH} t} \tag{10}$$

Where ϕ_l and $\psi_l$are the velocity and stream function, C_1 and C_2 are constants, I_0 and I_1 are modified Bessel functions of first kind, $L^2 = k^2 + w/\nu_l$. ν_l is the liquid kinematic viscosity.

With boundary conditions of liquid kinematic free surface, continuity of shear stress and continuity of normal stress, the dispersion relation has the form of Eq. (11).

$$\omega_{KH}^2 + 2\nu_l k_{KH}^2 \omega_{KH}\left[\frac{I_1'(k_{KH}r_p)}{I_0(k_{KH}r_p)} - \frac{2k_{KH}L}{k_{KH}^2+L^2}\frac{I_1(k_{KH}r_p)}{I_0(k_{KH}r_p)}\frac{I_1'(Lr_p)}{I_1(Lr_p)}\right] = \frac{\sigma k_{KH}}{\rho_l r_p^2}\left(1-k_{KH}^2 r_p^2\right)\left(\frac{L^2-r_p^2}{L^2+r_p^2}\right)\frac{I_1(k_{KH}r_p)}{I_0(k_{KH}r_p)} + \frac{\rho_g}{\rho_l}\Big(U - i\frac{\omega_{KH}}{k_{KH}}\Big)^2\left(\frac{L^2-r_p^2}{L^2+r_p^2}\right)\frac{I_1(k_{KH}r_p)}{I_0(k_{KH}r_p)}\frac{K_0(k_{KH}r_p)}{K_1(k_{KH}r_p)} \quad (11)$$

Numerical solutions for the maximum grow rate Ω_{KH}were generated and the solution is shown in Eq. (12).

$$\Omega_{KH}\left[\frac{\rho_l r_p^2}{\sigma}\right]^{0.5} = \frac{(0.34+0.38We_g^{1.5})}{(1+Z_l)(1+1.4T^{0.6})} \quad (12)$$

Where $T = Z_l\sqrt{We_g}$. Note that if $\omega_{KH}$is greater than Ω_{KH}, then breakup occurs.

The Rayleigh-Taylor analogy is based on the instability generated from rapid drop deceleration due to aerodynamic forces. This force is mathematical described as shown in Eq. (13). (Richards et al, 2016)

$$\left|\mathrm{F}_{D,i}\right| = \mathrm{M}_d|\mathrm{a}_i| = \mathrm{M}_d\frac{3}{8}\mathrm{C}_D\frac{\rho_g|\mathrm{U}_i|^2}{\rho_l r_0} \quad (13)$$

Where $|\mathrm{a}_i|$ is the acceleration of the drop, M_d is the mass of the droplet and C_D the drag coefficient. The fastest growing wavelength is shown in Eq. (14).

$$\Lambda_{RT} = 2\pi\sqrt{\frac{3\sigma}{a(\rho_l-\rho_g)}} \quad (14)$$

According to (Xin et al., 1998) if $\mathrm{C_{RT}}\Lambda_{\mathrm{RT}}$ is smaller the diameter of the droplet, where C_{RT} is a constant that predicts the radius of the breakup droplet, then waves are assumed to grow on the surface of the droplet. If these wavelengths grow for sufficient time, which depends on an adjustable constant, the breakup occurs.

2.3 LISA Spray Breakup Model

The linearized Instability sheet atomization (LISA) described by (Senecal et al., 1999)) breakup model described by (O'Rourke and Amsden, 1987) is based on the imposition of infinitesimal disturbances on a liquid sheet generated by the entrance of the viscous two-dimensional liquid in a quiescent chamber. The dispersion relation for a sinuous mode is derived considering that second-order viscosity terms can be neglected and also making the consideration of short waves *($tanh(kh) = 1 and\ Q \ll 1$)* by Eq. (15). (Richards et al, 2016)

$$w_r = -2\nu_l k^2 + \sqrt{4\nu_l{}^2k^4 + QU^2k^2 - \sigma k^3/\rho_l} \quad (15)$$

Where w_r is the real wave growth rate, k is the wave number, $\rho_g$is the gaseous specific mass, *U* is the sheet initial velocity, h is half of the sheet thickness and $Q = \rho_g/\rho_l$.

A critical Weber number *of* $We = \rho_g U^2 h/\sigma = 27/16$ was analytically derived. If the Weber number is below this critical value long waves are responsible for breakup, in the other hand if it is greater than the critical value short waves dominate the process. Assuming that Weber number is typically above the critical value the assumptions made to get in Eq. (15) are reasonable.

If a wave reaches a critical amplitude value, parts of the liquid breakup from the sheet to form drops. This maximum amplitude is related to a maximum wave growth rate Ω_S, derived from Eq. (15) represented in Eq. (16).

$$\Omega_S = \frac{V}{L}\ln\left(\frac{\eta_b}{\eta_0}\right) \quad (16)$$

Where the quantity $\ln(\frac{\eta_b}{\eta_0})$ is set to 12, V is the absolute velocity of liquid sheet and $\mathrm{L}^2 = \mathrm{k}^2 + \mathrm{w}/\nu_l$.

3. PHYSICAL MODEL

This chapter highlights both the experimental and the numerical methodologies.

3.1 Experimental procedure

The experimental apparatus is described by (Guzzo, 2012) as a quiescent chamber presented in Figure 6.

Figure 6 – Quiescent chamber (Guzzo, 2012)

To perform the experiment, the PIV technique was used as well as a high speed camera. The analysis of the pixels in the images was used to create a MalLab routine to define the angle of the spray. The break-up length was obtained by means of a luminosity analyse of the spray images obtained by the PIV technique. The images obtained by the high speed camera were used to obtain the spray penetration.

Figure 7 shows an image of a spray 1.15 ms after the beginning of the injection obtained with the high speed camera and its respective profile used to extract the cited information.

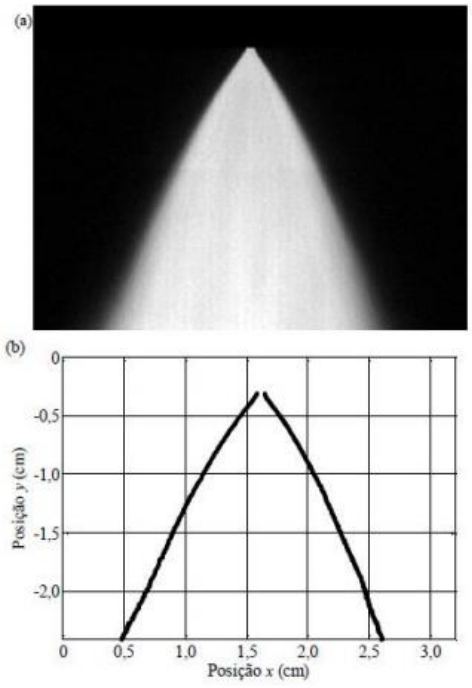

Figure 7 – Spray and its profile (Guzzo, 2017)

The main characteristics extracted from the experimental tests are show in Table 1. These data was used to simulate the spray in CONVERGE.

Table 1. Main characteristics of the spray. (Reis,2017)

Injector position (x,y,z) [m]	(0;0;0.012)
Injector direction (x,y,z) [m]	(0.0021;0;0.9999)
Injector hole [mm]	0.5628
Internal cone angle [^{0}]	41.5
External cone angle [^{0}]	63.0
Chamber temperature [K]	296
Chamber wall temperature [K]	296
Chamber pressure [Pa]	$1.01x10^5$
Injection time [ms]	1.5

More details about the experiments can be found in (GUZZO, 2012), (GUZZO M. E., 2017) and (GOMES JÚNIOR, 2017).

3.2 Numerical procedure

The computational domain, which represents the quiescent chamber is 100 mm height and has 70 mm of diameter. The surface mesh was created in the Convergent Science Inc.'s CONVERGETM CFD software. This software uses this surface mesh to generate a volumetric structured mesh in every time step. Figure 8 shows the surface mesh with an embedded region, illustrated in a green cone. This embedded region locally refines the volumetric mesh.

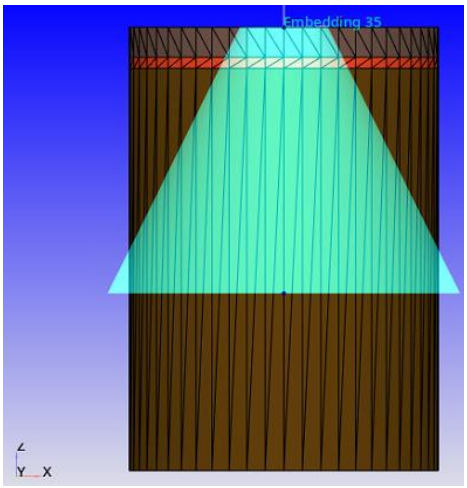

Figure 8 – Computational domain in CONVERGE

Figure 9 shows a cut plane in the centre of the domain, illustrating the volumetric mesh and the spray. The base mesh size is set to 3.6 mm. The embedded region illustrated in Figure 4 refines the mesh inside the cone in a scale of 2^n, in which *n* is set by the user, in the simulation n is set to 2 so that the base size of the cells has 0.9 mm. CONVERGE also allows a dynamic mesh refinement, in which the user can choose a parameter which will be tracked, if the value or the difference between the value of adjacent cells are greater than a pre-set value then the mesh is locally refined. In this simulation the speed of the liquid drops is set to be tracked, so that in the locations which the velocity is greater than a pre-set value the mesh is refined by a scale of 2^3. Figure 5 also shows this adaptive mesh refinement in cells near the drops (the drops are illustrated in blue in the upper centre of the image, and the mesh is shown in pink).

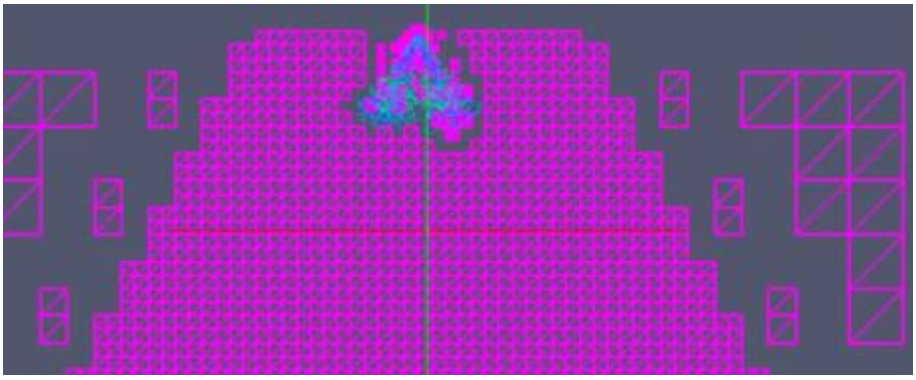

Figure 9 – Computational domain in PARAVIEW

The simulation treats the air phase as an Eulerian phase and the liquid as Lagrangian. The injected liquid is ethanol, which has specific mass of 797.5 [kg/m^3], dynamic viscosity of 1.11x10^{-3} [Pa s] and surface tension of 2.43x10^{-2} [N/m]. To model the turbulence for the Eulerian phase the RNG-ke model is used and the main parameters for the Lagrangian phase are shown in Table 2.

Table 2 – Main spray models

Spray model physical process	**Model**
Liquid injection	Hollow cone
Spray breakup	TAB, KHRT, LISA
Drop drag	Dynamic drag
Collision model	O'Rourke model
Collision outcomes model	O' Rourke
Drop turbulent dispersion	O'Rourke model
Drop /wall interaction	Rebound
Evaporation model	Multi-component vaporization

4. RESULTS AND DISCUSSION

The spray penetration is shown in Figure 10 for the different breakup models tested in comparison with the experimental data. It is noted that KH-RT and TAB model have a similar behavior but the LISA model predicts a greater penetration comparing with the other two models in the beginning of the simulation, but all three models converge to a similar value of maximum penetration. Comparing to the experimental data TAB and KH-RT models are well fitted inside the experimental limits until 1 ms of simulation overestimating the penetration for further times. The LISA model overestimates the penetration for 0.85 ms and so on.

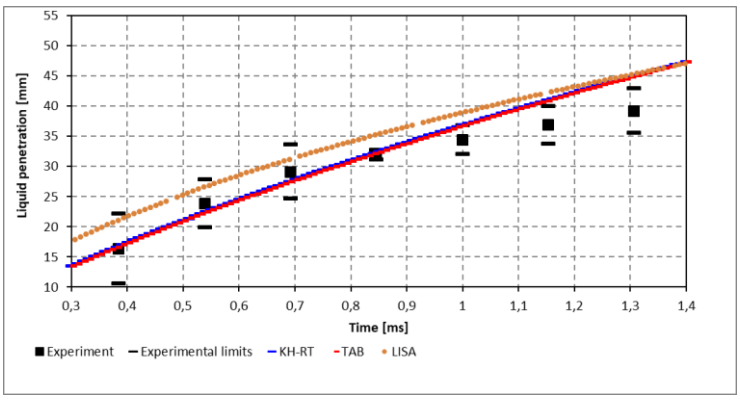

Figure 10 – Liquid penetration comparison

In Figure 11 the simulated spray is shown and in Figure 12 the same spray is shown side by side with the image generated by the experimental procedure, both by the time of 1.15 ms. In the images it is noted that the spray shape predicted by the simulation is similar to the experimental, but it is also observed in the images that the experimental image has a pre-spray which is caused by low injection pressure in the beginning of the process and it is represented in the image in the white concentration below the maximum diameter, it is important to clarify that the pre-spray is not considered in the penetration length. This pre-spray is not considered in the simulation, thus, it is not illustrated in the image.

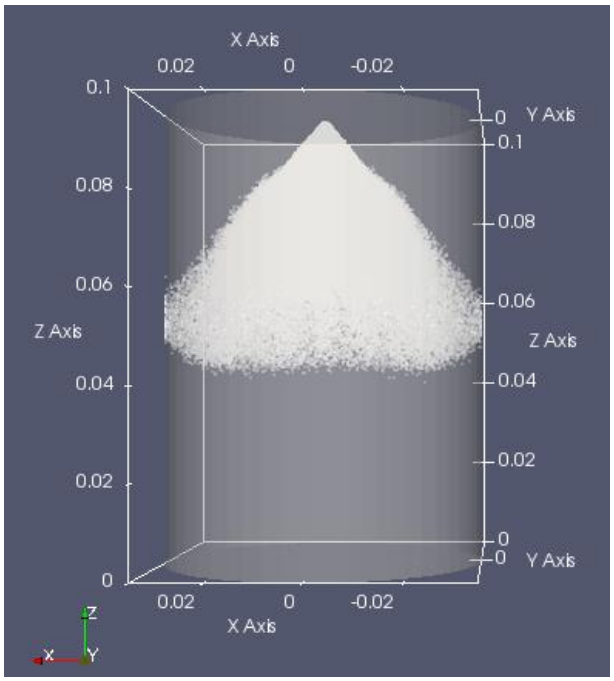

Figure 11 –Simulated spray in PARAVIEW for the KH-RT model

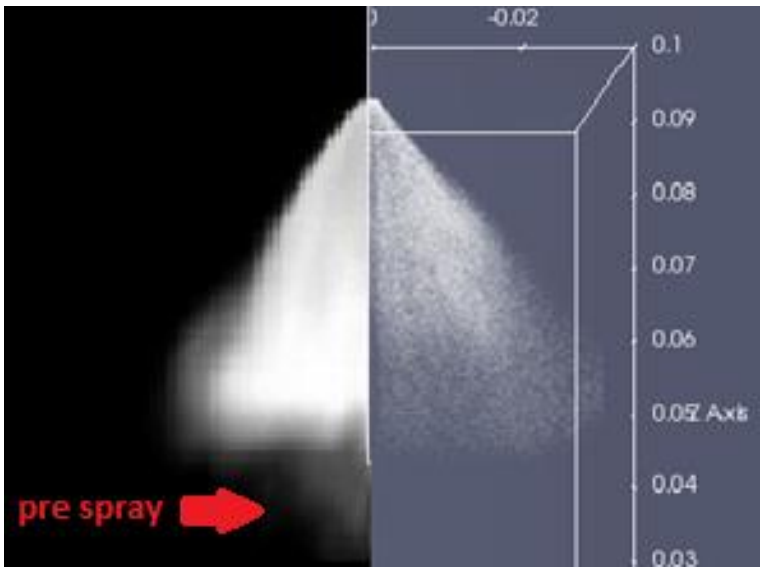

Figure 12 – Experimental image of the spray with the simulated spray in PARAVIEW for the KH-RT model

5. CONCLUSION

All the breakup models tested demonstrate good predictions of spray penetration, however they over predict this phenomenon. TAB and KH-RT are better fitted to the experimental data having a very similar behaviour while LISA model predicts greater values for spray penetration.

The images show that the simulation captured the shape of the spray besides the pre-spray, which is not considered in this simulation.

To achieve better results a model that considers the pre-spray needs to be developed and also check existing models in respect to the over predicting of penetration length.

6. ACKNOWLEDGMENTS

We would like to express gratitude to Convergent Science Inc. for their assistance and for the use of the CONVERGE™ software. Acknowledgement is given to Universidade Federal de Uberlândia for providing the computational resources used for the CFD simulation presented and for Programa de Pós-graduação em Engenharia Mecânica – FEMEC/UFU for fostering research activities. This study was financed in part by the Coordenação de Aperfeiçoamento de Pessoal de Nível Superior - Brasil (CAPES) - Finance Code 001.

7. REFERENCES

BAUMGARTEN, C., 2006. Mixture Formation in Internal Combustion Engines. s.l.:Springer Science & Business Media.

BRAVO, L. & KWEON, C. B., 2014. A review on liquid spray models for diesel engine computational analysis.. ARMY RESEARCH LAB ABERDEEN PROVING GROUND MD.

GOMES JÚNIOR, C. A., 2017. Análise da Influência da Pressão de Injeção, Contrapressão Ambiente e Tipo de Combustível nos Parâmetros da Atomização de um Injetor de Injeção Direta de Combustível High - Pressure Swirl.. s.l.:s.n.

GUZZO M. E., 2017. Desenvolvimento de Métodos Computacionais para Análise da Injeção Direta de Combustíveis Líquidos. s.l.:s.n.

GUZZO, M. E., 2012. Metodologias para Análise e Caracterização dos Sprays de um Injetor de Injeção Direta de Gasolina. s.l.:s.n.

GUZZO, M. E. et al., 2015. Experimental Characterization of Ethanol Sprays from a Single Hole Direct Injection Injector. SAE Technical Paper.

LEFEBVRE, A. H., 1989. Atomization and sprays. s.l.:Hemisphere Pub.

O'ROURKE, P. J., and Amsden, A. A., "The TAB Method for Numerical Calculation of Spray Droplet Breakup," SAE Paper No. 872089, 1987.

REIS, L. M. et al., 2017. Methodology for Numerical Simulations of a Mult-hole Injector With Experimental Validation. Acta Mechanìca Et Mobilitatem, Volume 2.

RICHARDS K. J., Senecal, P. K., and Pomraning, E., CONVERGE (Version 2.3) Manual, Convergent [Book]. - Middleton, WI : Science, Inc., 2016

REITZ, R., 1987. Modeling atomization processes in high-pressure vaporizing sprays.Atomisation and Spray Technology, Volume 3, pp. 309-337.

SENECAL, P. K., Schmidt, D. P., Nouar, I., Rutland, C. J., Reitz, R. D., and Corradini, M. L., "Modeling High-Speed Viscous Liquid Sheet Atomization," International Journal of Multiphase Flow, Volume 25, p. 1073, 1999.

XIN, J., Ricart, L., and Reitz, R. D., "Computer Modeling of Diesel Spray Atomization and Combustion," Combustion Science and Technology, Volume 137, p. 171, 1998.

8. RESPONSIBILITY NOTICE

The authors are the only responsible for the printed material included in this paper.